Nativa, Sinop, v. 9, n. 5, p. 612-627, 2021.
Pesquisas Agrárias e Ambientais
DOI: https://doi.org/10.31413/nativa.v9i5.13168 ISSN: 2318-7670

Solar radiation incidence under different shading screens in tropical climate: diurnal evolution and estimates

Daniela Roberta BORELLA[1], Hercules NOGUEIRA[2], Francielli Aloisio MORATELLI[3], Aline KRAESKI[3], Adilson Pacheco de SOUZA[1,2,3]

1 Postgraduate Program in Environmental Physics, Federal University of Mato Grosso, Cuiabá, MT, Brazil.
1 Institute of Agrarian and Environmental Sciences, Federal University of Mato Grosso, Sinop, MT, Brazil.
1 Postgraduate Program in Environmental Sciences, Federal University of Mato Grosso, Sinop, MT, Brazil.
*E-mail: drborella@gmail.com
(ORCID: 0000-0003-2941-2116; 0000-0001-7056-351X; 0000-0002-0304-985X; 0000-0001-5795-9245; 0000-0003-4076-1093)

Submitted on 11/17/2021; Accepted on 12/29/2021; Published on 12/30/2021.

ABSTRACT: The use of photoselective screens improves plant productivity and quality, and it is necessary to understand the dynamics of solar radiation transmissivity under these microenvironments to subsidize agricultural and forestry production projects. Therefore, the objective of this work was to describe the diurnal and seasonal evolution of incidence of global irradiance (I_G), photosynthetically active irradiance (I_{PAR}), and luminance in aboveground forest nurseries under different shading screens. Radiometric fractions were evaluated and statistical equations were obtained based on the external incidence. Instantaneous measurements of I_G, I_{PAR}, and luminance in the exterior and interior of nurseries (East-West direction), solstices (12/22/2018 and 06/20/2019) and equinoxes (03/21/2019 and 09/21/2019), and local zenithal culminations (02/18/2019 and 10/20/2019) were evaluated between 7h00min and 17h00min. Estimates were evaluated and the data were grouped into two databases composed of 70% and 30%, respectively, to generate and validate regressions for each variable. The statistical performance of regressions was evaluated using the following statistical indicators: coefficient of determination (R^2), mean square error (MSE), root mean square error (RMSE), and Willmott index (d). I_G, I_{PAR}, and luminance presented similar dynamics of diurnal and seasonal evolution under the shading screens for external conditions, and the transmissivity was affected by the environmental conditions (water seasonality and solar declination) and intrinsic characteristics of the shading screens (porosity and color). The transmission and absorption of I_G, I_{PAR}, and luminance were affected by color and porosity of the shading screens, whereas the reflection was affected only by the color. The values of Willmott index were higher than 0.9975 and 0.9973 for black screen and photoselective screen, respectively, and were considered as good, indicating that the equations generated good estimates of I_G, I_{PAR}, and luminance for application in different regions. The choice of shading screens for crops are dependent on spectral composition requirements and I_{PAR} transmissivity of each species.
Keywords: radiometric properties of photoselective screens; photosynthetically active radiation; irradiance; luminance; statistical indicators.

Radiação solar incidente sob diferentes telas de sombreamentos em clima tropical: evolução diurna e estimativas

RESUMO: O uso de telas foto-seletivas melhora a produtividade e qualidade das plantas, e é necessário compreender a dinâmica da transmissividade da radiação solar sob esses microambientes para subsidiar projetos de produção agrícolas e florestais. Nesse sentido, o objetivo foi descrever a evolução diurna e sazonal das irradiâncias global (I_G), fotossintéticamente ativa (I_{PAR}) e luminância incidentes em viveiros florestais suspensos sob diferentes telas de sombreamento. Além disso foram avaliadas as frações radiométricas e obtidas equações estatísticas de estimativas baseadas na incidência externa. As medidas instantâneas de I_G, I_{PAR} e luminância ocorreram no exterior e interior dos viveiros (alinhados no sentido Leste-Oeste), nos solstícios (22/12/2018 e 22/06/2019), equinócios (21/03/2019 e 21/09/2019) e nas culminações zenitais locais (18/02/2019 e 20/10/2019), entre às 7h00min e 17h00min. Para avaliação das estimativas, os dados foram agrupados em duas bases, compostas por 70 e 30% para geração e validação das regressões, para cada variável, respectivamente. Para avaliação do desempenho estatístico das regressões foram empregados os indicativos estatísticos: coeficiente de determinação (R^2), erro absoluto médio (MBE), raiz quadrada do erro quadrático médio (RMSE) e índice de Willmott (d). I_G, I_{PAR} e luminância apresentaram dinâmicas semelhantes na evolução diurna e sazonal sob as telas de sombreamento em relação as condições externas, sendo a transmissividade influenciados por condições ambientais (sazonalidade hídrica e declinação solar) e intrínsecas a tela (porosidade e cor). A transmissão e absorção de I_G, I_{PAR} e luminância foram afetadas pela cor e porosidade líquida, enquanto que a reflexão apenas pela cor. Os valores do índice de Willmott foram superiores a 0,9975 e 0,9973 para as telas pretas e foto-seletivas, respectivamente, sendo considerado como ótimos, indicando que as equações ajustadas permitem boas estimativas de I_G, I_{PAR} e luminância para aplicação em diferentes regiões. A escolha da tela de sombreamento para o cultivo de plantas fica dependente das necessidades de composição espectral e transmissividade da I_{PAR} de cada espécie.
Palavras-chave: propriedades radiométricas de telas foto-seletivas; radiação fotossinteticamente ativa; irradiâncias; luminância; indicadores estatísticos.

1. INTRODUCTION

Solar radiation is the main source of energy that regulates physical, biochemical, and physiological processes of earthly components; it determines the microclimate, mainly modulating temperatures, air humidity, and soil moisture, is responsible for energy exchanges in the water-soil-plant-atmosphere system, and is essential for ecophysiological responses of plants, which reflects in crop yields and product quality.

The availability of energy that reaches the earth surface is dependent on astronomical (solar declination), atmospheric (cloudiness, air humidity, and atmospheric turbidity), and geographical factors that determine spatial and temporal variations in solar radiation incidence (TERAMOTO et al., 2019). In addition, the atmosphere composition (gases, aerosols, water vapor, dust, and particulate matter) affects the transmissivity of solar radiation, and the clouds are the main reductors because they absorb specific wavelengths (infrared) and reflect and diffuse (anisotropically) most solar radiation (SOUZA, et al., 2016; PALÁCIOS et al., 2018).

The transitional region between the Cerrado and Amazon biomes in northern state of Mato Grosso, Brazil, has high mean monthly global radiation, from 16.56 ± 2.82 MJ m^{-2} day^{-1} (February, rainiest month in the region) to 21.17 ± 0.83 MJ m^{-2} day^{-1} (October), with higher atmospheric transmissivity and solar radiation in the dry season, between May and October (SOUZA et al., 2016). It is estimated that a fraction of this global radiation (40% to 45%) consists of photosynthetically active radiation (between 400 and 700 nm), which corresponds to a good part of the visible range of the electromagnetic spectrum (BERGAMASCHI; BERGONCI, 2017) and is responsible for activating photosynthetic process in plants (WANG et al., 2015; WU et al., 2019).

Excess or lack of solar radiation can be harmful to different groups of plant species; moreover, they affect flows of latent heat (evapotranspiration) and sensitive heat (air temperature) (AHMED et al., 2016). Direct incidence of global solar radiation on plants can cause significant changes to their biochemical, physiological, and morphogenic processes (ZHANG; ZHANG, 2017; WU et al., 2019), oxidative stress, compromised photosynthetic activity and structural and metabolic changes in chloroplasts are some of the damage caused by the combination of high light and heat stress (BALFAGÓN et al., 2019).Therefore, the use of protected environments for agricultural crops and forest species in regions of adverse climate conditions has been increasingly studied, focused on improving yields and quality of species that present difficulties for production in specific seasons of the year or regions (HOLCMAN; SENTELHAS, 2012; AHMED et al., 2019; TANG et al., 2020; BORELLA et al., 2020a).

The use of white plastic screens in greenhouses with artificial or natural ventilation (AHMED et al., 2019), in nebulization or evaporative cooling systems (AHMED et al., 2016), and in energy system with solar photovoltaic modules (TANG et al., 2020) predominates among the protected crop systems. However, other plastic materials with different physical characteristics (chemical composition, porosity, color, and density) have been used alone or combined with plastic screens (KOTILAINEN et al., 2018; CHOAB et al., 2019).

Some ecophysiological studies have investigated microclimate dynamics and effects of using photoselective screens (aluminized or thermo reflectors, red, blue, green, and black) on the growth and development of plants and found promising results (HOLCMAN; SENTELHAS, 2012; MONTEIRO et al., 2016; MAHMOOD et al., 2018; SABINO et al., 2020; BORELLA et al., 2020a,b). Nevertheless, a better understanding of microclimate dynamics in these protected environments is important for different regions and seasons of the year, since the choosing of the adequate type of screen and percentage of shading (porosity) is dependent on the species, cultivar, and local climate conditions (ABDEL-GHANY, 2015; AHMED et al., 2016; STATUTO et al., 2020).

Information on micrometeorological dynamics within protected environments is essential for the planning and development of hydro-agricultural activities, crop management, and selection of agricultural and forest species better adapted to local environmental conditions, focusing on reducing costs, saving water, and increasing production.

The use of shading screens in hot regions decreases the harmful effects caused by high irradiance on plants (AHMED et al., 2016; ZHANG; ZHANG, 2017; BORELLA et al., 2020b), providing a more uniform distribution of temperature and relative air humidity under shaded environments (AHMED et al., 2019; BORELLA et al., 2021), reducing the water vapor pressure deficit (CHOAB et al., 2019) and, consequently, the water demand of plants (MONTEIRO et al., 2016; BORELLA et al., 2020a). In addition, it forms a physical protection barrier against insects-pest (MAHMOOD et al., 2018). Thus, shading is a simple and low-cost method regarding implementation and maintenance (ABDEL-GHANY et al., 2015).

However, controlling climate variables in these environments is a complex and dynamic process that depends on external conditions (HOLCMAN; SENTELHAS, 2012) and a monitoring routine. Moreover, the implementation costs of monitoring routine systems with sensors and data acquisition systems (dataloggers) can be high. Thus, micrometeorological information under protected environments with no sensors can be obtained by using simplified statistical models based on weather variables under full-sun environmental conditions and that allow the estimation of a variable of interest, such as solar radiation, with a high degree of accuracy (SOUZA et al., 2017; ROSSI et al., 2018; TERAMOTO et al., 2019).

Therefore, the objectives of this work were to describe the diurnal and seasonal evolution, determine the radiometric ratios, and fit statistic models for estimating global irradiance (I_G), photosynthetically active irradiance (I_{PAR}), and luminance (Lux) through shading screens with different physical and spectral characteristics. The evaluations were carried out in different crop seasons, in a tropical climate region of Brazil, to obtain tools to subsidize agricultural and forest production projects.

2. MATERIAL AND METHODS

2.1. Study region and implementation

The study was conducted in a transitional region between the Cerrado and Amazon biomes, in Sinop, Mato Grosso (MT), Brazil (11°51'50"S, 55°29'08"W and 384 meters of altitude). The region presents an Aw climate (tropical hot and wet), according to the Köppen classification (SOUZA et al.,

2013), with mean annual air temperature and relative air humidity of 25.9 °C and 74.0%, respectively (Figure 1A and 1B). The mean daily global radiation and insolation of the region are 17.5 to 21.2 MJ m^{-2} day^{-1} and 8.2 to 9.7 hours day^{-1} in the dry season, and 16.8 to 18.6 MJ m^{-2} day^{-1} and 4.9 to 6.3 hours day^{-1} in the rainy season (Figure 1C).

The climate seasonality of the region is defined by two hydrological seasons: rainy (October to April) and dry (May to September) (Figure 1D) (SOUZA et al., 2013). The mean annual rainfall depth is 1,945.0 mm, which is more than 1,700.0 mm in the spring-summer season, whereas the reference evapotranspiration range is from 105.0 to 170.0 mm $month^{-1}$ (3.5 to 5.5 mm day^{-1}) between the rainy and dry periods in the region (Figure 1D).

The solar radiation components were measured in aboveground forest nurseries arranged in an East-West direction, with dimensions of 3.0 × 1.0 × 1.0 m (length, width, and height), and at 1.0 m above the ground. The full-sun conditions were used as reference; the top, front, and lateral sides of the experimental units were covered with black polyolefin screens with 35%, 50%, 65%, and 80% shading, thermo-reflector screen (Aluminet®, 50% shading), and red, blue (Chromatinet®, 50% shading) and green (Frontinet®, 50% shading) polyolefin screens.

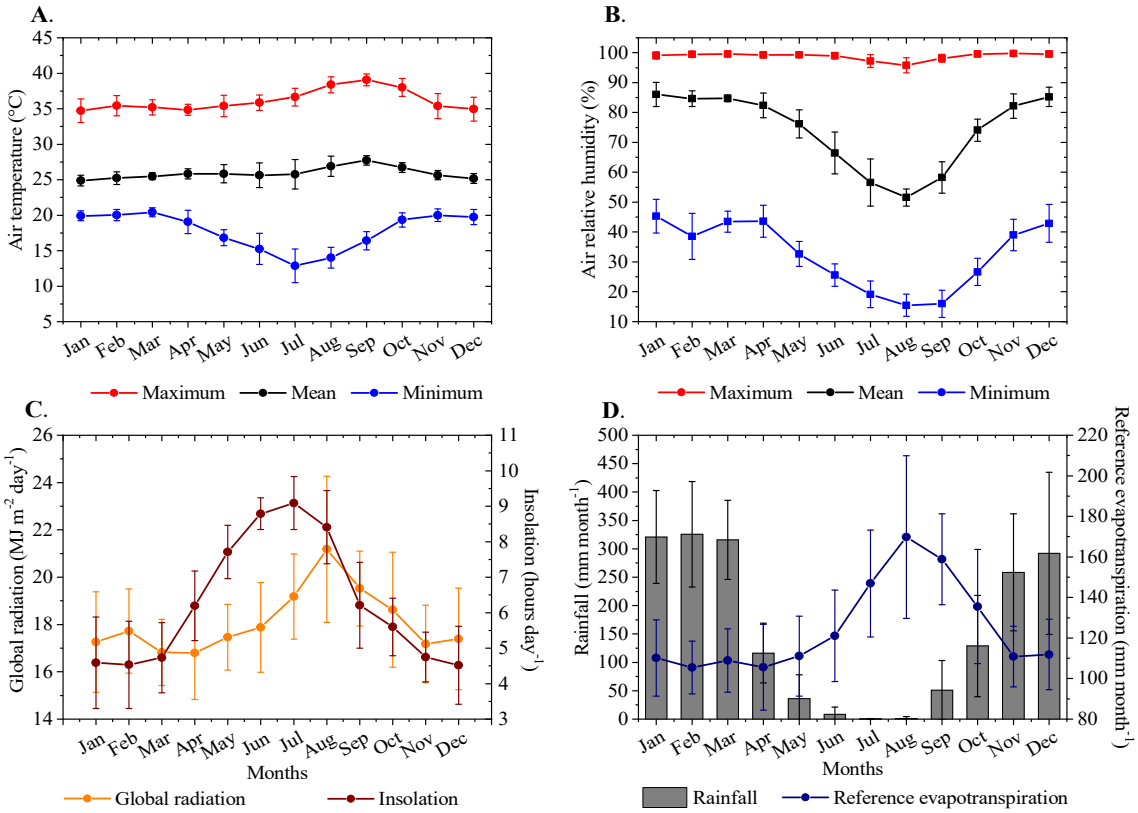

Figure 1. Monthly means and standard deviations for air temperature (A), relative air humidity (B), global radiation and insolation (C), rainfall and reference evapotranspiration (D) between September 01, 2010 and December 31, 2019 in Sinop, MT, Brazil.
Figura 1. Médias mensais e desvio-padrão da temperatura do ar (A), umidade relativa do ar (B), radiação global e insolação (C), precipitação e evapotranspiração de referência (D), entre 01/09/2010 e 31/12/2019, em Sinop, MT, Brasil.

2.2. Measurements of I_G, I_{PAR}, and Luminance

Instantaneous measurements of incident and reflected global irradiance (I_G – W m^{-2}), photosynthetically active irradiance (I_{PAR} – µmol m^{-2} s^{-1}), and luminance (lux) were measured in the protected environments (nurseries) covered with shading screens and in the environments at full-sun conditions. The following sensors were used: i) pyranometer MP-200 (spectral reading range of 360 to 1,120 nm; directional response (cosine effect): 5% up to 75° of zenith angle; temperature response; -0.04 ± 0.04% per °C; response time: minimum of 1.0 m s^{-1}; non-linearity: below 1% for measures above 1,750 W m^{-2}); ii) pyranometer MQ-200 (spectral reading range: 410 to 655 nm (considering a maximum of 50% wavelengths in this range); directional response (cosine effect): 5% up to 75° of zenith angle; temperature response; 0.06 ± 0.06% per °C; response time: minimum of 1.0 m s^{-1}; non-linearity: below 1% for measures above 3,000 µmol m^{-2} s^{-1} of Apogee; and iii) lux meter (LD-200 - Instrutherm). These sensors were fixed in a leveled metal platform at 1.50 m height inside and at 0.50 m above each unit (aboveground nursery).

Solar radiation was measured in the summer solstice (December 22, 2018) and winter solstice (June 22, 2019), when the solar declination (δ) is equal to -23.45 and 23.45°; in the autumnal equinox (March 21, 2019) and spring equinox (September 21, 2019), when δ = 0°; and in the local zenithal culmination (ϕ -11.85°) on February 18, 2019 and October 20, 2019, between 7h00min and 17h00min (local solar time), in external (above) and internal (inside) conditions of each aboveground nursery, with maximum intervals of 2 minutes from each other to minimize the hour angle effects. Three readings (replications) were carried out for each time of the day, date, and protected environment.

The data were analyzed for consistency, and different values were excluded due to reading errors generated by the data acquisition system or by atmospheric instability (cloudy sky), as the case of some times in September and October. The irradiance at the top of the atmosphere (I_0) was obtained and, then, the coefficient of atmospheric transmissivity (K_T) was determined by the ratio between global irradiance (I_G) and irradiance at the top of the atmosphere (I_0).

The transmissivity of I_G, I_{PAR}, and luminance under the polyolefin screens were obtained by the ratio between readings of the variable inside and outside the protected environments. The percentage of transmission, reflection, and absorption of the irradiances were calculated based on the incident and reflected data found for each shading screen.

2.3. Statistical models to estimate I_G, I_{PAR}, and luminance

The hourly instantaneous values of I_G, I_{PAR}, and luminance in shading conditions were grouped into two databases: one with 70% of the total data for calibration of statistical coefficients of models (with dates of December 22; March 21; September 21, and October 20), and other with 30% of the data for validation of statistical performance of estimation models (with the dates of February 18 and June 22). Simple linear regressions (y = a + b x) were used between internal I_G, I_{PAR}, and luminance (dependent variable) and external I_G, I_{PAR}, and luminance (independent variable) for each shading condition.

The statistical performance of the generated models was evaluated using the following indicators: mean square error (MSE) (Eq. 1), root mean square error (RMSE) (Eq. 2) and fit of the Willmott index (dw) (Eq. 3) (SOUZA et al., 2017).

$$\mathrm{MSE} = \frac{\sum_{i=1}^{n}|P_i - O_i|}{n} \quad (01)$$

$$RMSE = \left[\frac{\sum_{i=1}^{n}(P_i - O_i)^2}{n}\right]^{0.5} \quad (02)$$

$$dw = 1 - \frac{\sum_{i=1}^{n}(P_i - O_i)^2}{\sum_{i=1}^{n}(|P'_i - \bar{O}| + |O'_i - \bar{O}|)^2} \quad (03)$$

where: P_i is the estimated values; O_i is the measured values; n is the number of observations; $|P'_i|$ is the absolute value of the difference $P'_i - \bar{O}$; and $|O'_i|$ is the absolute value of the difference $O'_i - \bar{O}$.

The fractions of I_{PAR} and luminance (independent variable) in relation to I_G (variable dependent) were determined using linear regressions with grouping of data from black screens with different porosities and from photoselective screens with the same porosity.

3. RESULTS

The atmospheric conditions in the zenithal culmination dates for the latitude -11.85° are presented in the Table 1. There was 0.2 mm rainfall at the evening of October 20, 2019, when the atmospheric transmissivity was lower than 0.35, i.e., a cloudy sky (ESCOBEDO et al., 2009). This atmospheric condition hindered the instantaneous measurements of I_G, I_{PAR}, and luminance between 15h00min and 17h00min in that date (Figures 2 to 4K-L).

Table 1. Daily rainfall, air temperature, relative air humidity, global radiation, and insolation in different dates of solar declination, in Sinop, MT, Brazil.
Tabela 1. Valores diários de precipitação, temperatura do ar, umidade relativa do ar, radiação global e insolação nas diferentes datas de declinação solar, em Sinop, MT, Brasil.

Date	Rainfall	Air temperature (°C)			Relative air humidity (%)			Global radiation	Insolation
	(mm)	Mean	Maximum	Minimum	Mean	Maximum	Minimum	(MJ m^{-2} d^{-1})	(hours)
12/22/2018	0	27.55	36.50	21.50	71.19	95.00	34.00	18.67	7.10
02/18/2019	0	25.81	32.46	21.56	83.50	99.20	49.94	20.85	9.30
03/21/2019	0	26.20	33.29	22.23	87.10	97.72	60.81	14.65	5.00
06/22/2019	0	29.94	34.66	20.43	46.80	94.94	32.94	17.65	10.40
09/21/2019	0	28.35	38.97	22.45	63.87	94.94	32.94	15.72	5.80
10/20/2019	0.2	27.49	35.74	22.35	71.98	94.90	39.70	17.74	5.30

3.1. Diurnal and seasonal evolution of solar radiation through shading screens

The global and photosynthetically active irradiances and the luminance presented similar dynamics throughout the day, regardless of the microenvironment (full-sun conditions and under shading screens) and the different solar declinations for the same latitude (-11.85°). The highest peaks of incidence of solar radiation occurred by 12h00min and the lowest at sunrise and sunset, 07:00 and 17h00min, respectively (Figures 2, 3, and 4), due to variations in the zenith angle.

The highest incident energy levels in full-sun conditions at approximately the solar mid-day (I_G > 1000 W m^{-2}, I_{PAR} > 2000 μmol m^{-2} s^{-1}, and luminance > 60.000 lux) were found during the rainy season, in the summer solstice, autumnal equinox, and at the local solar culmination, whereas the lowest energy levels were found in the dry and dry-rainy seasons (winter solstice and spring equinox, respectively).

The increase in black polyolefin screen shading level gradually decreased the I_G, I_{PAR}, and luminance inside the microenvironments in all dates (declinations) considered in this study. Contrastingly, in the qualitative analysis, the black polyolefin screen, thermo-reflector screen, and red, blue, and green polyolefin screens, all with 50% shading, presented similar I_G transmissivity values; a higher transmissivity of I_{PAR} and luminance was found for the black polyolefin screen when compared to the other colored screens with the same shading percentage (Figures 3 and 4).

3.2. Solar radiation transmission, reflection, and absorption through shading screens

The values of coefficient of atmospheric transmissivity (K_T) of global radiation ranged from 0.43 in October to 0.69 in February (rainy season), and from 0.67 in June to 0.54 in September (dry season), confirming the results of Souza et al. (2016), who found intervals of monthly K_T ranging from 0.43

to 0.56 in the rainy season and from 0.54 to 0.64 in the dry season, for this same region. The variations in mean daily global radiation (Table 1) and K_T (Table 2) found for the evaluation dates (February 18, 2019 and October 20, 2019), corresponding to zenithal culmination and the period rainy season, were strongly affected by atmospheric instability (cloudiness) at the time of the instantaneous measurements.

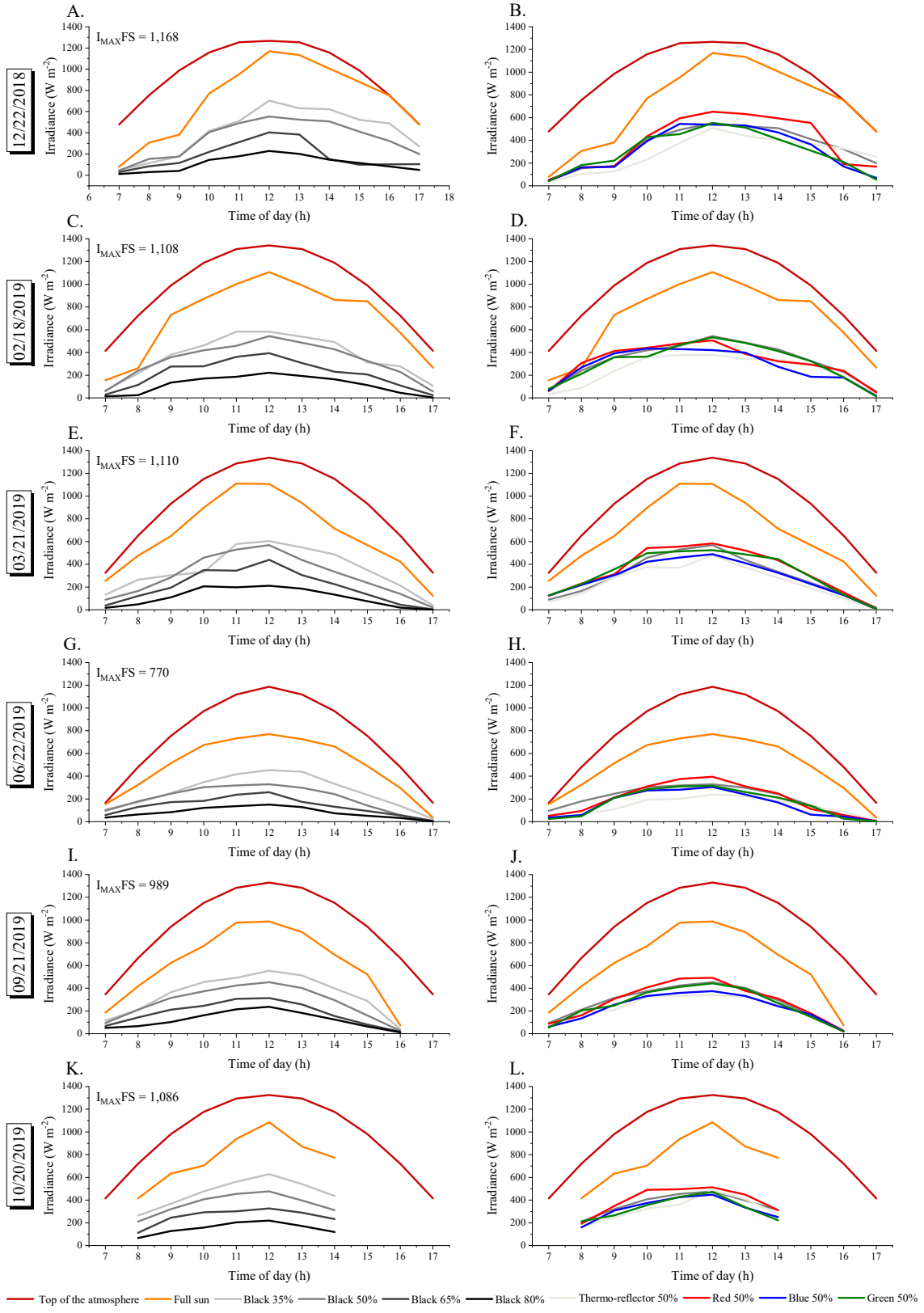

Figure 2. Diurnal and seasonal evolution of irradiance at the top of the atmosphere and global irradiance under increasing levels of shading (left) and spectral solar radiation (right), in Sinop, MT, Brazil.
Figura 2. Evolução diurna e sazonal das irradiâncias do topo da atmosfera e global sob níveis crescentes de sombreamento (à esquerda) e espectrais (à direita) da radiação solar, em Sinop, MT, Brasil.

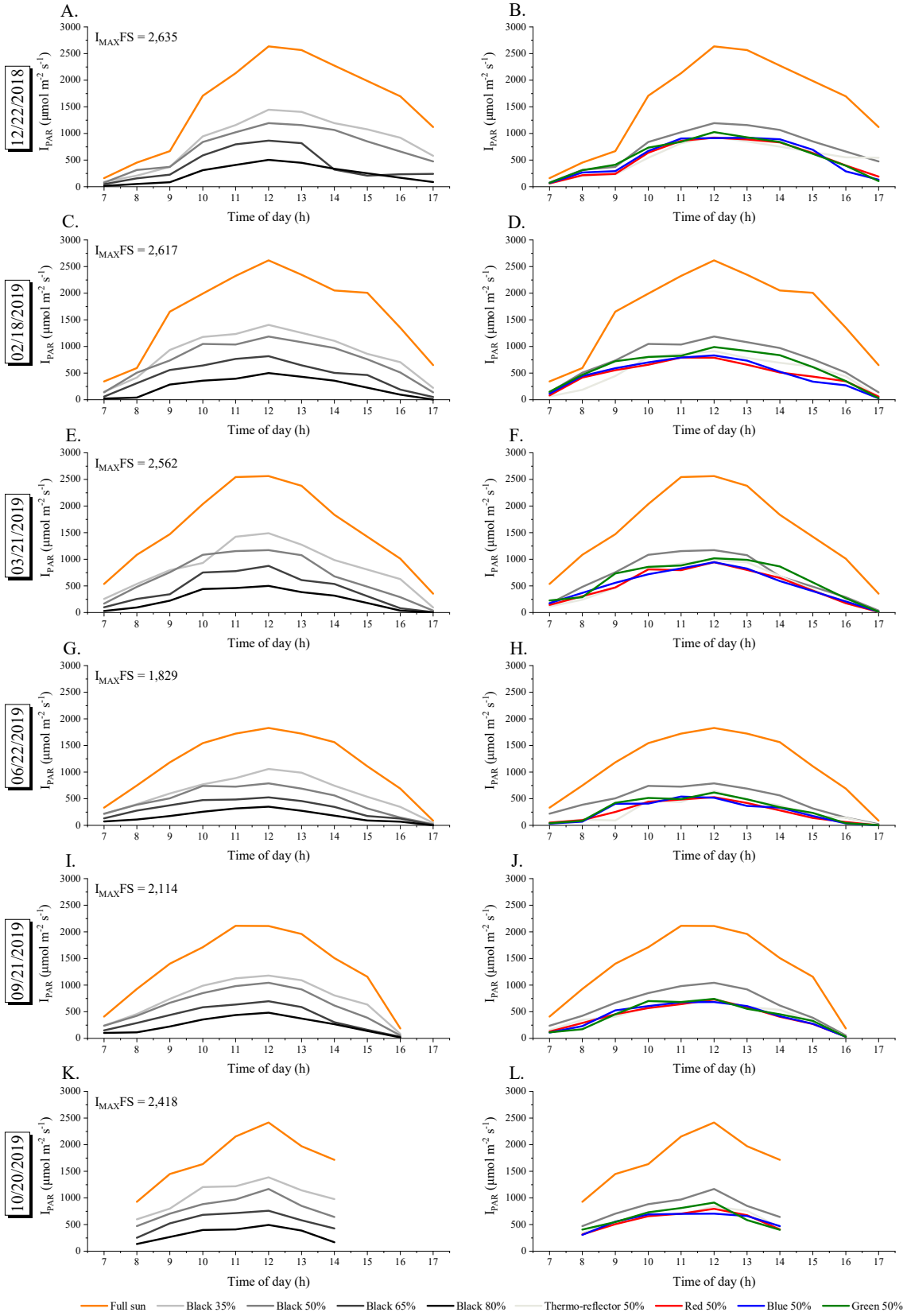

Figure 3. Diurnal and seasonal evolution of photosynthetically active irradiance under increasing levels of shading (left) and spectral solar radiation (right), in Sinop, MT, Brazil.
Figura 3. Evolução diurna e sazonal da irradiância fotossintéticamente ativa sob níveis crescentes de sombreamento (à esquerda) e espectrais (à direita) da radiação solar, em Sinop, MT, Brasil.

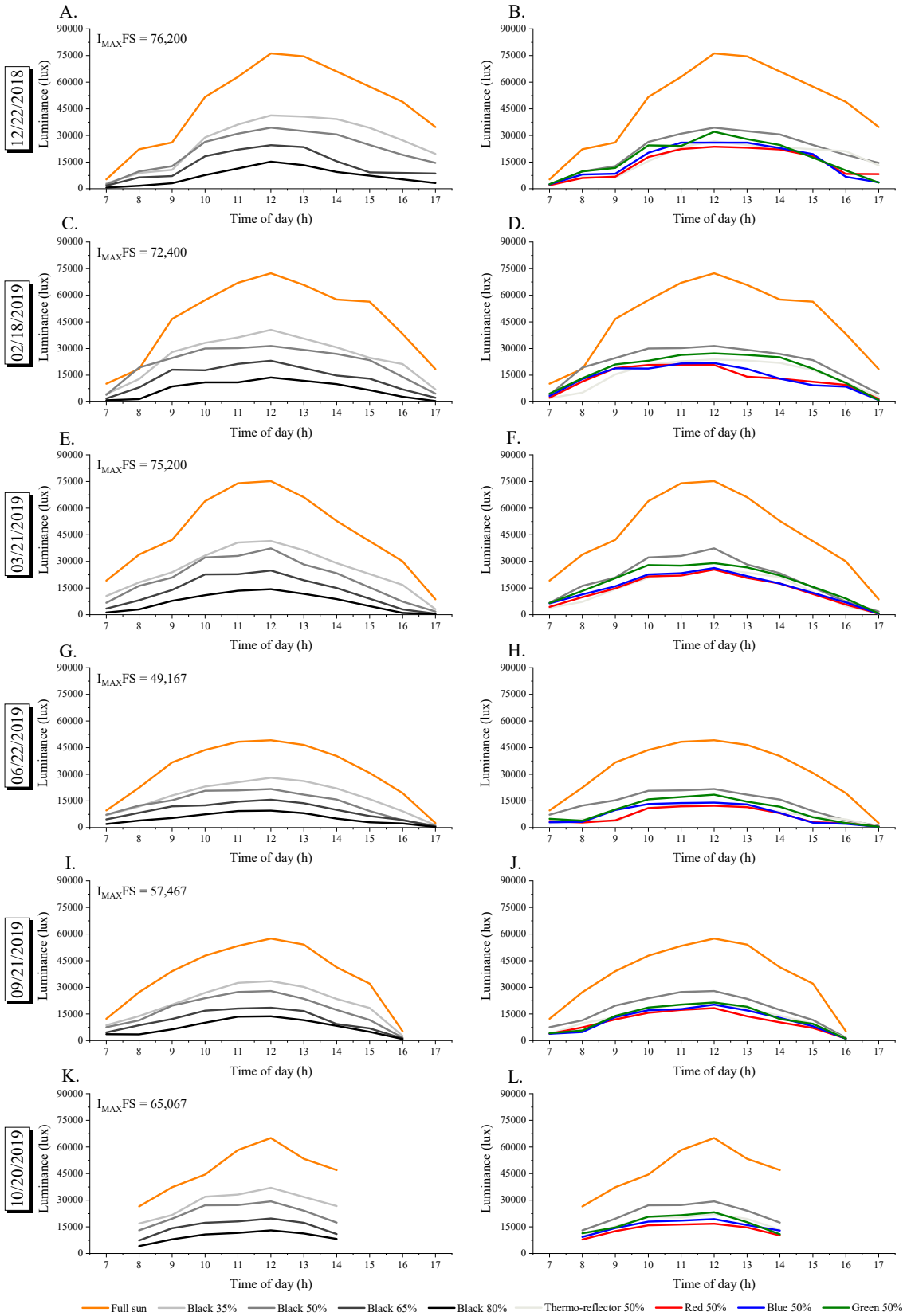

Figure 4. Diurnal and seasonal evolution of luminance under increasing levels of shading (left) and spectral solar radiation (right), in Sinop, MT, Brazil.

Figura 4. Evolução diurna e sazonal da luminância sob níveis crescentes de sombreamento (à esquerda) e espectrais (à direita) da radiação solar, em Sinop, MT, Brasil.

The transmissivity of I_G, I_{PAR}, and luminance found for the protected environments covered with black polyolefin screens of 35%, 50%, 65%, and 80% shading decreased as the shading level was increased, regardless of the solar declination. Consequently, the increase in shading level decreased the transmission and reflection due to the increase in absorption of I_G, I_{PAR}, and luminance (Table 2 and Figure 5).

Regarding the photoselective (colored) screens with 50% shading, the mean transmissivities of irradiance were 0.4216, 0.3169, 0.3250, 0.3210, and 0.3524 for the black, thermo-reflector, red, blue, and green screens, respectively. Black screen with 50% shading presented higher transmission (42.16%) and lower reflection (4.23%) of I_G, I_{PAR}, and luminance than thermo-reflector, red, blue, and green screens, except for the I_G in the red screen in (44.00%).

The thermo-reflector screen (as commercially described) presented the highest reflection (22.50%) and the lowest absorption, regardless of the season. The red screen presented the lowest absorbed I_G (34.29%); contrastingly, it was the screen that presented the highest absorption levels of I_{PAR} and luminance, together with the blue screen.

Table 2. Daily mean values of coefficients of transmission, reflection, and absorption of solar irradiance in polyolefin screens in relation to atmospheric conditions in different dates of solar declination, in Sinop, MT, Brazil.
Tabela 2. Valores médios diários dos coeficientes de transmissão, reflexão e absorção das irradiâncias solares de telas poliefinas com relação à condição atmosférica nas diferentes datas de declinação solar, em Sinop, MT, Brasil.

Date	K_T	$K_{Tt35\%}$	$K_{Tt50\%}$	$K_{Tt65\%}$	$K_{Tt80\%}$	$K_{Tttr50\%}$	$K_{Ttvm50\%}$	$K_{Ttaz50\%}$	$K_{Ttvd50\%}$
Global radiation									
12/22/2018	0.72	0.55	0.45	0.25	0.14	0.39	0.48	0.47	0.43
02/18/2019	0.69	0.53	0.43	0.28	0.14	0.35	0.46	0.39	0.44
03/21/2019	0.70	0.50	0.37	0.25	0.13	0.31	0.44	0.39	0.43
06/22/2019	0.67	0.51	0.39	0.27	0.15	0.28	0.36	0.29	0.30
09/21/2019	0.54	0.55	0.43	0.28	0.19	0.34	0.42	0.34	0.37
10/20/2019	0.43	0.57	0.45	0.32	0.19	0.38	0.47	0.39	0.39
Transmission	0.6240	0.5368	0.4215	0.2743	0.1575	0.3402	0.4399	0.3792	0.3944
Reflection	-	0.0726	0.0569	0.0478	0.0473	0.2559	0.2172	0.1507	0.1121
Absorption	-	0.3907	0.5216	0.6778	0.7951	0.4039	0.3429	0.4701	0.4935
Photosynthetically active radiation									
12/22/2018	-	0.51	0.43	0.24	0.14	0.34	0.30	0.36	0.35
02/18/2019	-	0.53	0.42	0.27	0.13	0.32	0.30	0.30	0.38
03/21/2019	-	0.50	0.36	0.23	0.12	0.28	0.26	0.28	0.34
06/22/2019	-	0.50	0.38	0.25	0.13	0.24	0.20	0.21	0.23
09/21/2019	-	0.52	0.43	0.26	0.17	0.31	0.28	0.27	0.28
10/20/2019	-	0.56	0.44	0.30	0.17	0.32	0.30	0.31	0.33
Transmission	-	0.5226	0.4111	0.2602	0.1429	0.2999	0.2737	0.2889	0.3186
Reflection	-	0.0405	0.0302	0.0273	0.0279	0.2065	0.1002	0.0534	0.1740
Absorption	-	0.4369	0.5587	0.7125	0.8292	0.4936	0.6261	0.6577	0.5074
Luminance									
12/22/2018	-	0.53	0.44	0.26	0.14	0.35	0.28	0.34	0.37
02/18/2019	-	0.54	0.44	0.28	0.14	0.33	0.29	0.30	0.40
03/21/2019	-	0.52	0.40	0.26	0.13	0.28	0.27	0.31	0.37
06/22/2019	-	0.52	0.43	0.30	0.16	0.24	0.20	0.22	0.28
09/21/2019	-	0.55	0.45	0.29	0.19	0.32	0.26	0.28	0.31
10/20/2019	-	0.57	0.45	0.30	0.19	0.34	0.27	0.31	0.34
Transmission	-	0.5376	0.4322	0.2810	0.1577	0.3105	0.2613	0.2949	0.3443
Reflection	-	0.0480	0.0397	0.0367	0.0357	0.2123	0.0884	0.0564	0.0674
Absorption	-	0.4144	0.5281	0.6822	0.8066	0.4773	0.6503	0.6488	0.5883

where: K_T is the coefficient of atmospheric transmissivity; $K_{Tt35\%}$, $K_{Tt50\%}$, $K_{Tt65\%}$, $K_{Tt80\%}$, $K_{Tttr50\%}$, $K_{Ttvm50\%}$, $K_{Ttaz50\%}$, and $K_{Ttvd50\%}$ are coefficients of transmissivity for black polyolefin screens with 35%, 50%, 65%, and 80% shading, and thermo-reflector, red, blue, and green screens, respectively.
em que: K_T é o coeficiente de transmissividade atmosférica; $K_{Tt35\%}$, $K_{Tt50\%}$, $K_{Tt65\%}$, $K_{Tt80\%}$, $K_{Tttr50\%}$, $K_{Ttvm50\%}$, $K_{Ttaz50\%}$ e $K_{Ttvd50\%}$ são os coeficientes de transmissividade das telas poliefinas pretas de 35, 50, 65 e 80% de sombreamento, termorefletora, vermelha azul e verde, respectivamente.

3.3. Estimates of I_G, I_{PAR}, and luminance under the shading screens

The linear regressions used to estimate I_G, I_{PAR}, and luminance under the protected environments covered with polyolefin screens presented coefficients of determination (R^2) higher than 80% for the three variables and in all shading screens evaluated (Figures 6 and 7).

In general, the equations used for the estimates under screens black presented underestimates (negative MSE values), however, lower than 1% of the mean values for each variable. The black screens with 50% and 65% shading presented the highest deviations and, consequently, higher spreading (RMSE) for the estimates of the three irradiances (Figure 6). In the thermo-reflector, blue, and red screens, the equations generated overestimates (positive MSE values), except for I_G and I_{PAR} in the red screen and for all irradiances in the green screen. The spreading (RMSE) was observed in estimates for the 50% thermo-reflector screen (Figure 7). The Willmott index was higher than 0.9975 and 0.9973 for the black and photoselective screens, respectively.

The mean fractions of I_{PAR} and luminance in relation to I_G in the black screens with increasing shading levels were 44.80% and 1.55%, respectively (Figures 8A, B). The fractions of irradiance in the black screens were similar, thus, they were not presented separately in this study. In general, these fractions for photoselective screens were approximately 52.60 and 1.85% (Figure 8C, D); however, when analyzed separately, it presented variations in fractions of I_{PAR} (44.88 to 68.70%) and luminance (1.56 to 2.62%) from the black to the red screen (Table 3).

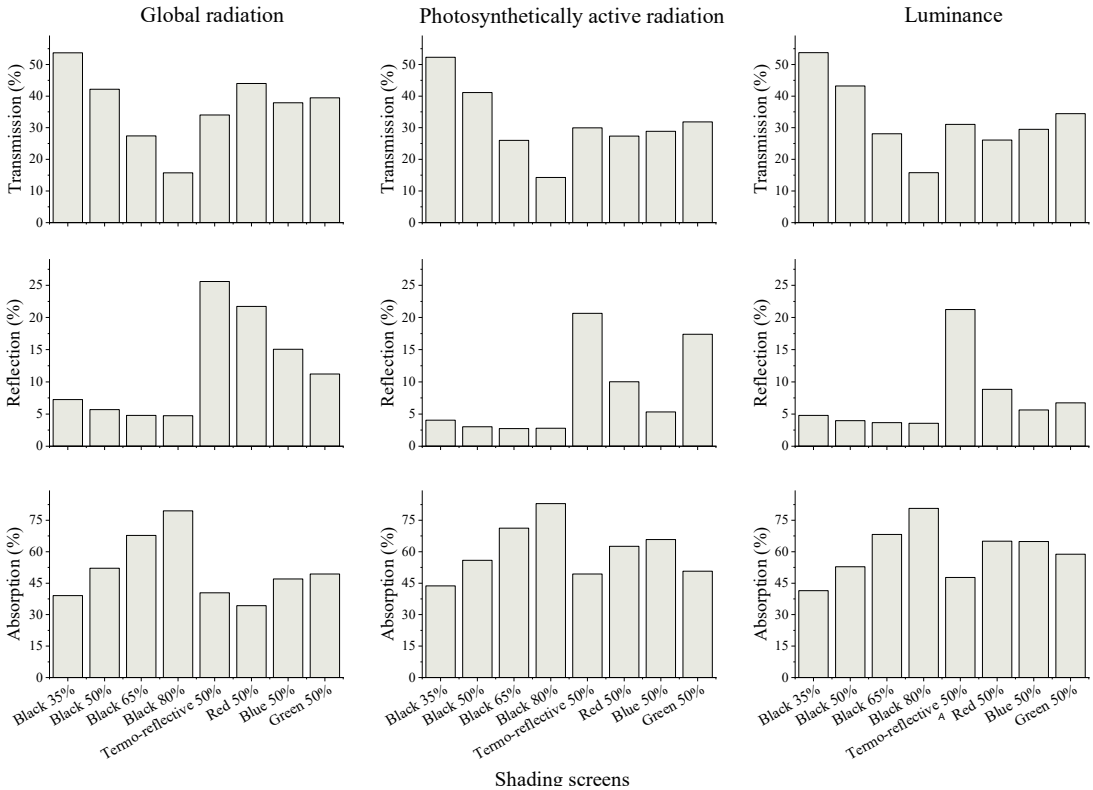

Figure 5. Percentage of transmission, reflection, and absorption of global and photosynthetically active radiations and luminance under different shading screens, in Sinop, MT, Brazil.

Figura 5. Percentuais de transmissão, reflexão e absorção da radiação global, radiação fotossinteticamente ativa e luminância sob diferentes telas de sombreamento, em Sinop, MT, Brasil.

Table 3. Linear equations to estimate fractions of photosynthetically active radiation (I_{PAR}) and luminance in relation to global solar radiation (I_G) for photoselective screens, in Sinop, MT, Brazil.

Tabela 3. Equações lineares de estimativas da fração da radiação fotossinteticamente ativa (I_{PAR}) e da luminância em relação a radiação solar global (I_G) nas telas foto-seletivas, em Sinop, MT, Brasil.

Shading screen	Variables	Linear equations	Correlation coefficient (R^2)
Black 50%	I_{PAR}	$I_G = 0.44876\ I_{PAR}$	0.99586
	Luminance	$I_G = 0.01559$ luminance	0.99425
Thermo-reflector 50%	I_{PAR}	$I_G = 0.48248\ I_{PAR}$	0.9839
	Luminance	$I_G = 0.01711$ luminance	0.98765
Red 50%	I_{PAR}	$I_G = 0.68695\ I_{PAR}$	0.99215
	Luminance	$I_G = 0.02616$ luminance	0.98719
Blue 50%	I_{PAR}	$I_G = 0.55929\ I_{PAR}$	0.9938
	Luminance	$I_G = 0.02014$ luminance	0.99525
Green 50%	I_{PAR}	$I_G = 0.53496\ I_{PAR}$	0.99038
	Luminance	$I_G = 0.01825$ luminance	0.99209

4. DISCUSSION

The I_G, I_{PAR}, and luminance presented similar dynamics in the diurnal and seasonal evolution under the shading screens in relation to environmental conditions (full sun). In the diurnal evolution, the highest peak of incidence of these irradiances occurred at approximately the solar mid-day due to the lower angle of incidence (zenith angle) of solar rays on the surface, increasing the availability of energy per unit of area (BERGAMASCHI; BERGONCI, 2017).

The inflections of transmissivity values found approximately at sunrise and sunset occur due to the predominance of diffuse radiation (fraction of radiation not measured in this study). The plastic screens present similar radiometric properties to those of translucid materials (plastic), presenting a high transmittance of diffuse radiation, although the structure of plastic materials is not homogeneous (AL-HELAL; ABDEL-GHANY, 2010).

The temporal evolution of global irradiance follows the irradiance variations at the top of the atmosphere, and the seasonality is affected by solar declination and atmospheric dynamics (TERAMOTO et al., 2019). The highest transmissivity and fluctuations of I_G, I_{PAR}, and luminance occurred during the rainy season (summer-autumn), which is connected to the cloudiness dynamics at this latitude and season of the year. In this case, atmospheric instability occurs during the rainy season because of a high cloud density and water vapor concentration, reducing global radiation by reflection, absorption, and diffusion before it reaches the ground surface, which decreases the direct incidence of global radiation and indicates predominance of diffuse

radiation (ZAMADEI et al., 2021). This anisotropic dynamics of interaction of solar radiation with the atmosphere makes only a part of the solar radiation to be transmitted to the ground surface (SOUZA et al., 2016), thus explaining the fluctuations of I_G, I_{PAR}, and luminance under full-sun conditions and under shading screens over the day and the year (Figures 2 a 4).

Larger number of days with atmospheric transmissivity higher than 55% (open sky days with predominance of direct radiation) and lower oscillations of global radiation occur in the dry season (ZAMADEI et al., 2018) and, consequently, lower photosynthetically active radiation and luminance. However, the low atmospheric transmissivity and insolation found on September 21 (Tables 1 and 2) can be explained by the high concentration of aerosols present in the atmosphere due to high indexes of fires that occur during the dry season in the region (PALÁCIOS et al., 2018).

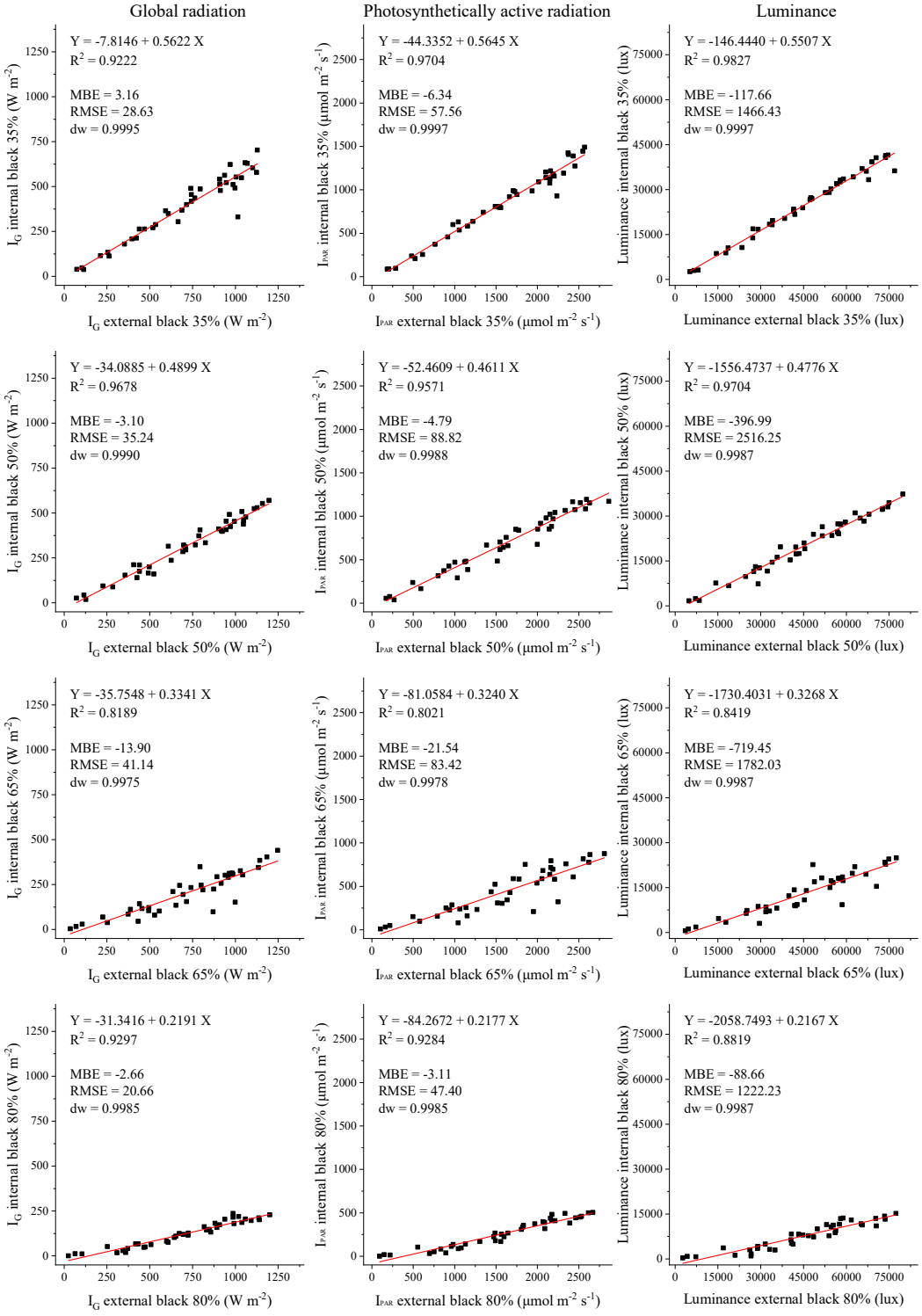

Figure 6. Linear equations for the estimates and their statistical indicators of global irradiance (I_G) photosynthetically active irradiance (I_{PAR}), and luminance under black polyolefin screens with different shading levels, in Sinop, MT, Brazil.
Figura 6. Equações lineares de estimativas e seus indicadores estatísticos das irradiâncias global (I_G), fotossinteticamente ativa (I_{PAR}) e luminância, sob telas poliefinas pretas com diferentes níveis de sombreamento, em Sinop, MT, Brazil.

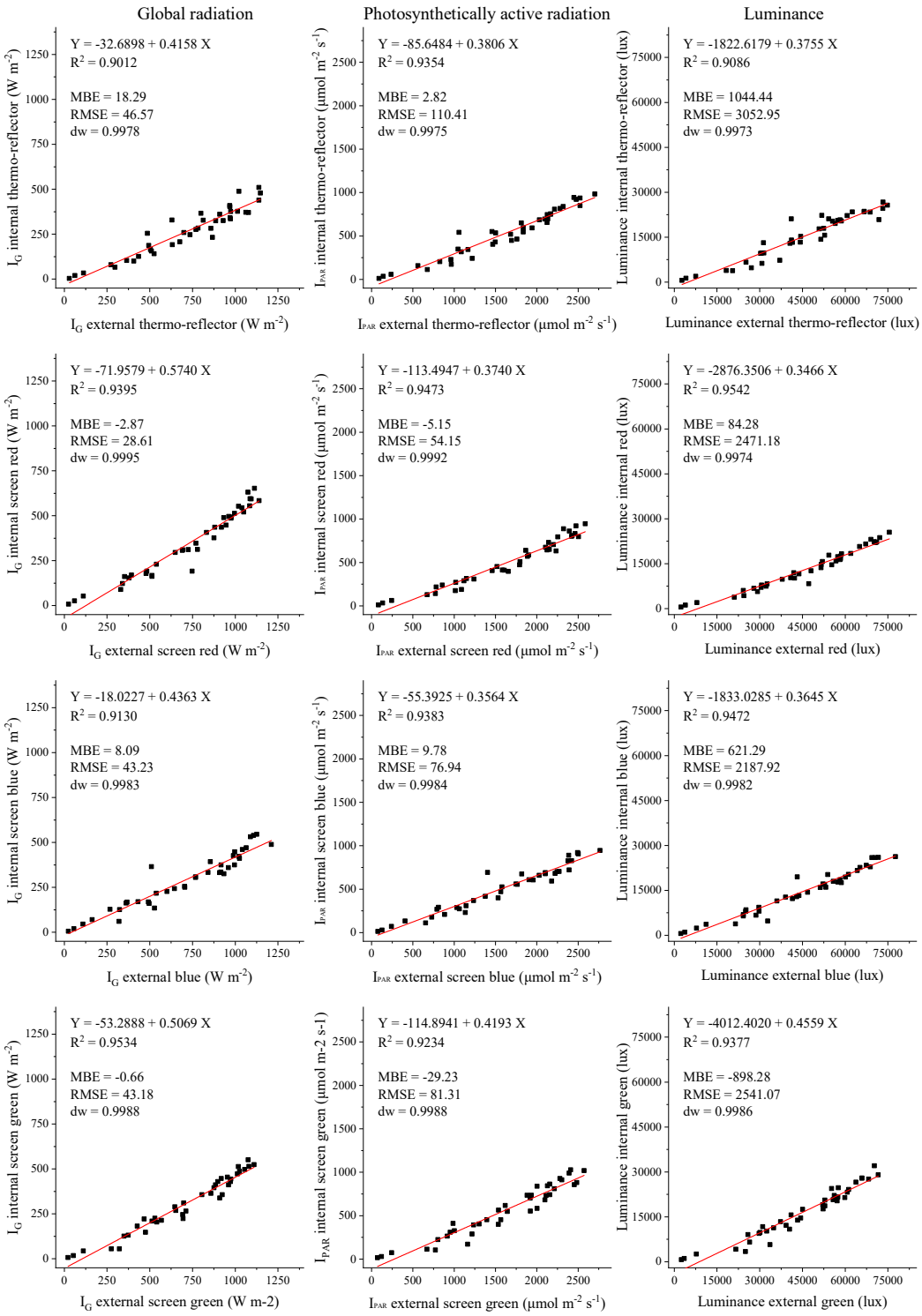

Figure 7. Linear Equations for the estimates and their statistical indicators of global irradiance (I_G), photosynthetically active irradiance (I_{PAR}), and luminance under photoselective polyolefin screens with 50% of shading, in Sinop, MT, Brazil.
Figura 7. Equações lineares de estimativas e seus indicadores estatísticos das irradiâncias global (I_G), fotossintéticamente ativa (I_{PAR}) e luminância, sob telas poliefinas foto-seletivas com 50% de sombreamento, em Sinop-MT.

In general, the intensity and distribution of solar radiation on the earth surface can be affected by factors in global scale (atmosphere composition, structure, and interaction, solar declination, and zenith angle) and regional scale (seasons of the year, latitude, altitude, slope, land position, atmosphere optical thickness, vegetation, soil, and continentality) (BERGAMASCHI; BERGONCI, 2017).

Global radiation interacts with materials in the Earth's surface, generating different dynamics of their properties that, combined with atmospheric effects, latitude, and season of the year, affect the seasonality of the incident and available radiation. Among these surface physical characteristics, The structure size, shape, position, and architecture, the material composition, porosity, roughness, texture, angle of exposure, aging, and degradation, the shading screen color and bright and radiometric property, and the water and dust deposited on the material also affect the transmission, reflection, and

absorption of solar radiation under shading screens (ABDEL-GHANY et al., 2015; CHOAB et al., 2019).

The spectral transmittance of black screens with different shading levels or porosity was directly proportional the screens porosity (Figure 5). Thus, the direct passage of solar radiation by the screen pores is dependent on its porosity (AL-HELAL; ABDEL-GHANY, 2010). Given the same porosity of the photoselective screens, the black screen presents higher transmittance than the other screens, denoting the higher effect of the screen color over the porosity on the transmittance of I_G, I_{PAR}, and luminance.

Similar dynamics of spectral transmittance were found under environmental conditions by Al-Helal; Abdel-Ghany (2010) and Sabino et al. (2020). Holcman; Sentelhas (2012) and Abdel-Ghany et al. (2015) found lower transmission for H_G and H_{PAR} in colored screens of same porosity under greenhouse conditions (Table 4). In addition to the strong effect of the solar radiation incidence angle and color and porosity of plastic screens (AL-HELAL; ABDEL-GHANY, 2010), the configuration of the structure and local climate can significantly reduce or increase the solar radiation transmissivity (MAHMOOD et al., 2018).

The reflectance of I_G, I_{PAR}, and luminance on the black screens with different porosities were low and proportional to the shading level; the opposite was found for the photoselective screens with similar porosities, since in this case, thermo-reflector, red, blue, and green screens presented higher reflectance than the black screen (Figure 5).

Higher reflectance of I_{PAR} were found for the thermo-reflector and green screens. The same result was reported by Al-Helal; Abdel-Ghany (2010) and Abdel-Ghany et al. (2015) (Table 4). Abdel-Ghany et al. (2015) reported that the high reflectance of solar radiation, combined with high absorption and emission of infrared thermal radiation (86.6%) of thermo-reflector screens, makes this material very useful to improve the energy balance of a greenhouse.

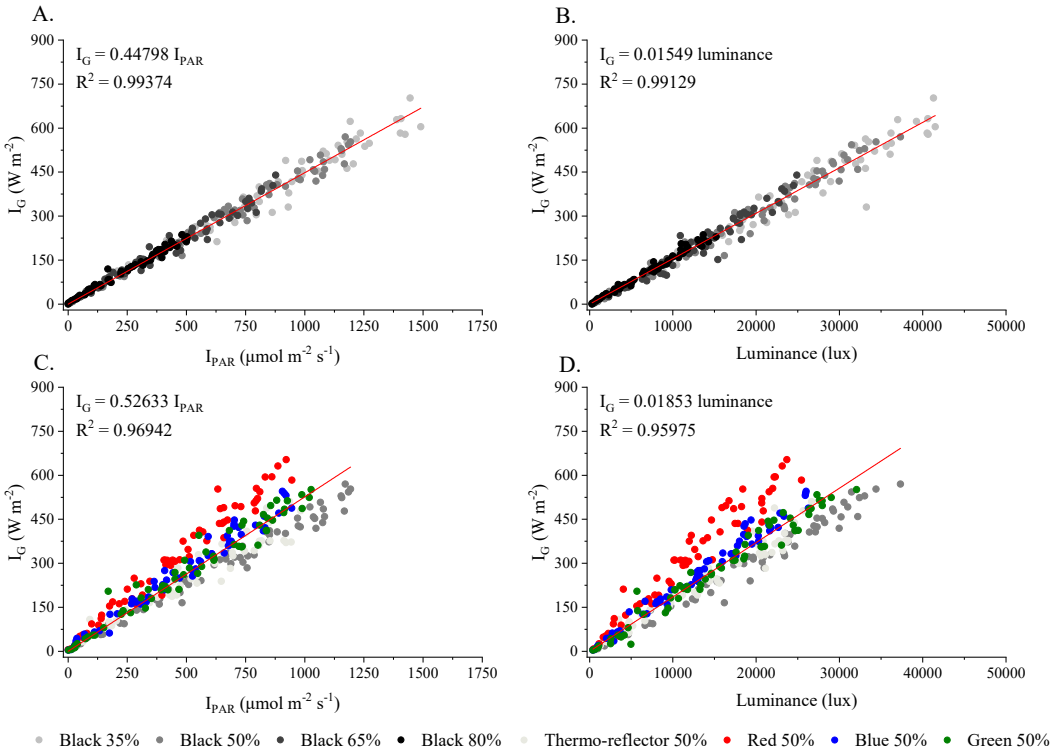

Figure 8. Linear equations for the estimates of fraction of photosynthetically active irradiance (I_{PAR}) and luminance in relation to global solar irradiance (I_G) under black screen (A and B) and photoselective screen (C and D).

Figura 8. Equações lineares de estimativas da fração da radiação fotossintéticamente ativa (I_{PAR}) e da luminância em relação a radiação solar global (I_G) nas telas pretas (A e B) e foto-seletivas (C e D).

According to Al-Hela; Abdel-Ghany (2010), the color brightness of shading screens has more effect on reflectance than its porosity, because a bright color screen reflects most of the incident H_{PAR}, i.e., the electromagnetic waves in this spectrum range, whereas a dark color screen reflects the incident H_{PAR} only on the screen color spectrum band and absorbs the incident H_{PAR} in the complementary remaining color spectrum.

The absorptions of I_G, I_{PAR}, and luminance by black shading screens were inversely proportional to the screen porosity. Abdel-Ghany et al. (2015) found that black screens with 70% shading in a greenhouse present approximately 68% absorption of H_G and H_{PAR}, since plastic screens with dark colors and lower porosity significantly increase the solar radiation absorption capacity, mainly the photosynthetically active radiation.

Considering a same porosity, red and blue screens present higher I_{PAR} absorption capacity, which is more than 10% when compared to the other screens; whereas thermo-reflector and green screens reflected 10% more I_{PAR} than the other screens. The color and brightness of plastic screens had significant effects on transmission, reflection, and absorption of I_G, I_{PAR} and luminance. Al-Helal; Abdel-Ghany (2010) found that most transmitted and reflected photosynthetically active radiation may have origin in the spreading of the screen texture, which depends on the color. Solar radiation

absorption also depends on the incident solar energy flow and radiation incidence angle on the target (BERGAMASCHI; BERGONCI, 2017).

The H_{PAR} represents 40% to 45% of the H_G, varying according to the atmospheric conditions (mainly cloudiness) and to the incidence angle, which varies according to the season of the year, latitude, and hour of the day (BERGAMASCHI; BERGONCI, 2017). The increase in the shading level of black screens decreased the quantity, but not the quality of the I_{PAR} transmitted by the screens, reaching approximately 45% internal I_G (Figure 8). The screen color affected considerably the proportion of I_{PAR} and luminance inside the I_G. The red screen (68.70%) presented more of 20% in the proportion of the I_{PAR} for the black screen (44.88%) and thermo-reflector screen (48.25%) and 13% more than the blue (55.93%) and green screens (53.50%) (Table 3).

Holcman; Sentelhas (2012) found proportions of 30%, 29%, 20%, and 17% of H_{PAR} on the H_G in black, thermo-reflector, red, and blue screens, respectively, all those with 70% shading under greenhouse conditions. The quality of radiation is the variation of distribution of radiant energy in different wavelengths; this variation occurs with the use of different colors and textures of plastic materials as shading (ABDEL-GHANY et al., 2015).

Table 4. Percentage of transmission, reflection, and absorption of radiation components by different shading screens, obtained in a literature review, for different places and periods of the year.
Tabela 4. Percentuais de transmissão, reflexão e absorção de componentes da radiação por diferentes telas de sombreamento obtidas em revisão de literatura, para diferentes localidades e períodos do ano.

Localization	Estructure	Shading screen	Transmission (%)	Reflection (%)	Absorption (%)	literature review
Saudi Arabia/Arid climate (BWh) - Latitude 24° 39' N and longitude 46° 47' E (December/2008 at February/2009) Winter	Full sun and oriented in a East-West direction.	Black 50%	47.0 H_{PAR}	8.0 H_{PAR}	45.0 H_{PAR}	Al-Helal and Abdel-Ghany (2010)
		Green 50%	43.0 H_{PAR}	11.0 H_{PAR}	46.0 H_{PAR}	
		Dark green 80%	19.0 H_{PAR}	6.0 H_{PAR}	75.0 H_{PAR}	
		Blue 80%	29.0 H_{PAR}	10.0 H_{PAR}	61.0 H_{PAR}	
Brazil/Subtropical climate (Cwa) - latitude 22° 42' 40" S, longitude 47° 37' 30" W and altitude of 546 m (December/2005 at June/2006) Summer and Autumn	Greenhouse covered with transparent low-density polyethylene (LDPE) of thickness 0.15 mm.	Black 70%	10.4 H_G 7.0 H_{PAR}			Holcman and Sentelhas (2012)
		Thermo-reflective 70%	13.6 H_G 8.4 H_{PAR}			
		Red 70%	27.0 H_G 12.0 H_{PAR}			
		Blue 70%	22.9 H_G 8.8 H_{PAR}			
Saudi Arabia/Arid climate (BWh) - Latitude 24° 39' N and longitude 46° 47' E (18 at 26 of December/2014) Winter	Greenhouse covered with polycarbonate sheet of 8.15 mm thickness and oriented in a North-South direction.	Black 70%	26.1 H_G 26.6 H_{PAR}	3.5 H_G 3.7 H_{PAR}	68.6 H_G 68.8 H_{PAR}	Abdel-Ghany et al. (2015)
		Thermo-reflective 85%	13.4 H_G 12.8 H_{PAR}	55.2 H_G 55.4 H_{PAR}	18.7 H_G 18.3 H_{PAR}	
Brazil/tropical hot and humid climate (Aw) - Latitude 11.85°S, longitude 55.56°W and altitude of 371m (July/2015 at April/2016) From Winter to Autumn	Full sun and oriented in a North-South direction.	Black 35%	62.2 Luminance 62.1 H_G 53.2 H_{PAR}			Sabino et al., (2020)
		Black 50%	44.6 Luminance 42.4 H_G 43.4 H_{PAR}			
		Black 65%	26.6 Luminance 28.8 H_G 27.8 H_{PAR}			
		Black 80%	13.0 Luminance 14.3 H_G 11.2 H_{PAR}			
		Thermo-reflective 50%	27.1 Luminance 38.1 H_G 35.4 H_{PAR}			
		Red 50%	27.2 Luminance 45.9 H_G 28.2 H_{PAR}			
		Blue 50%	23.0 Luminance 34.0 H_G 24.6 H_{PAR}			
		Green 50%	27.9 Luminance 34.5 H_G 27.4 H_{PAR}			

According to Kotilainen et al. (2018), the spectral composition (spectral quality) and fraction of reduced irradiation are strongly affected by color, porosity, and texture of shading screens. These authors found that black screens (35%, 50%, 70%, and 80% shading) do not change the quality of light in relation to the environmental solar light; contrastingly, the spectral quality (UVB 280-315 nm; GRAPE 315-400 nm; Blue 400-500 nm; Green 500-600 nm; Red 600-700 nm; Far-red 700-800 nm; NIR 800-900 nm) is affected by the color and porosity of shading screens.

The radiometric properties of plastic screens, combined with different local weather conditions, season of the year, and latitude, are responsible for transmission, reflection, and absorption of solar radiation; these materials directly affect the radiation balance inside protected microenvironments and, consequently, modify the microclimate (ABDEL-GHANY et al., 2015).

The transmitted solar radiation is retained and better used for physical processes in the radiation balance, saving energy (AHMED et al., 2016) and decreasing the irrigation water consumption (MONTEIRO et al., 2016; BORELLA et al., 2020a), benefiting the plant physiological performance (ZHANG; ZHANG, 2017) and production quality (KOTILAINEN et al., 2018).

Solar radiation affects other weather elements, mainly temperature (T_{ar}) and relative air humidity (UR_{ar}). The use of shading screens significantly decreases the sensitive heat in subtropical climate (HOLCMAN; SENTELHAS, 2012) and acts as a thermal insulation, decreasing heat loss in cold regions, mainly during the night (AHMED et al., 2016). In tropical climate regions under different water regimes, shading results in a higher uniformity of T_{ar} and UR_{ar} values for black and photoselective screens (BORELLA et al., 2021).

In addition, the radiation retained by the shading screens is reemitted as thermal radiation, generating a significant and more homogeneous increasing in mean values of T_{ar} and UR_{ar} under protected environments in tropical climate regions, mainly when covered with photoselective screens (BORELLA et al., 2021).

These dynamics of T_{ar} and UR_{ar} are due to convective exchanges of energy for a lower volume of air inside these shading environments, which contributes to a uniform distribution of temperature and relative air humidity in the vertical and horizontal extracts (AHMED et al., 2019) in different regions (STATUTO et al., 2020) and seasons of the year (BORELLA et al., 2021).

Considering these discussions, the appropriate choice of shading materials for crop plants is dependent on their characteristics regarding transmittance, spectral composition, temperature and relative air humidity dynamics, and water savings, associated with the ecophysiological requirements of each plant species.

The angular coefficient of the regressions fitted for the black screens decreased as the shading level was increased (Figure 6); thus, the proportion of incident solar radiation inside and outside the protected environment depends on the shading level provided by the polyolefin screens. This was not found for I_{PAR} and luminance in the thermo-reflector, red, blue, and green screens (Figure 7) because of the screen color and, probably, the texture on the transmissivity of I_{PAR}.

The coefficients of determination (R^2) of the regressions fitted for I_G, I_{PAR}, and luminance for the black and photoselective screens showed that more than 80% of the dependent variable (incident solar irradiance inside the protected environment) is connected to the independent variable (incident solar irradiance outside the protected environment) (Figures 6 and 7). This is a good correlation, despite 20% of the effect of external factors, as atmospheric conditions (ZAMADEI et al., 2018) and radiometric properties of plastic screens (ABDEL-GHANY et al., 2015).

These factors also induced under and overestimates of deviations (MSE) and spreads (RMSE) of the measures. However, they denote good performance of the equations, with Willmott indexes (d) above 0.9973, which is satisfactory.

5. CONCLUSIONS

The diurnal and seasonal evolution of global irradiance (I_G), photosynthetically active irradiance (I_{PAR}), and luminance under shading screens follow the atmospheric dynamics and are dependent on water seasonality and solar declination of the region and on radiometric properties, such as color and porosity of screens.

The transmission and absorption of I_G, I_{PAR}, and luminance are affected by color and porosity, and the reflection is affected by the shading screen color. The arrangement and structure also affect the energetic properties under these materials.

The simple linear regression statistical model is adequate to estimate I_G, I_{PAR}, and luminance under protected environments covered with black or photoselective shading screens with different porosities when the irradiances are measured under external environmental conditions.

The choice of shading screen for the planning and developing of agricultural crops and forests depends on information on the energetic needs of each species, the spectral quality and transmissivity of photosynthetically active radiation, and local external microclimate.

6. ACKNOWLEDGEMENTS

The authors thank the Brazilian Coordination for the Improvement of Higher Education Personnel (CAPES; Financing code 001); and the Brazilian National Council for Scientific and Technological Development (CNPq) for the scientific initiation and productivity scholarships (Process 308784/2019-7).

7. REFERENCES

ABDEL-GHANY, A. M.; PICUNO, P.; AL-HELAL, I.; ALSADON, A.; IBRAHIM, A.; SHADY, M. Radiometric Characterization, Solar and Thermal Radiation in a Greenhouse as Affected by Shading Configuration in an Arid Climate. **Energies**, v. 8, p. 13928-13937, 2015. DOI: 10.3390/en81212404

AHMED, H. A.; AL-FARAJ, A. A.; ABDEL-GHANY, A. M. Shading greenhouses to improve the microclimate. energy and water saving in hot regions: A review. **Scientia Horticulturae**, v. 201, p. 36-45, 2016. DOI: 10.1016/j.scienta.2016.01.030

AHMED, H. A.; YU-XIN, T.; QI-CHANG, Y.; AL-FARAJ, A. A.; ABDEL-GHANY, A. M. Spatial distribution of air temperature and relative humidity in the greenhouse as affected by external shading in arid climates. **Journal of Integrative Agriculture**, v. 18, n. 12, p. 2869-2882, 2019. DOI: 10.1016/S2095-3119(19)62598-0.

AL-HELAL, I. M.; ABDEL-GHANY, A. M. Responses of plastic shading nets to global and diffuse PAR transfer:

Optical properties and evaluation. **NJAS - Wageningen Journal of Life Sciences**, v. 57, p. 125-132, 2010. DOI: 10.1016/j.njas.2010.02.002

BALFAGÓN, D.; SENGUPTA, S.; GÓMEZ-CADENAS, A.; FRITSCHI, F.B.; AZAD, R.K.; MITTLER, R.; ZANDALINAS, S.I Jasmonic Acid Is Required for Plant Acclimation to a Combination of High Light and Heat Stress. **Plant Physiology**, v. 181, n. 4, p. 1668-1682, 2019. DOI: 10.1104/pp.19.00956

BERGAMASCHI, H.; BERGONCI, J. I. **As plantas e o clima: princípios e aplicações**. Guaíba: Agrolivros. 2017. 352p.

BORELLA, D. R.; SOUZA, A. P. de; SILVA, A. C. da; PIZZATTO, M.; KEFFER, J. F.; LIMA, D. C. Water requirements of *Dipteryx alata* Vogel Seedlings at different solar radiation levels in Cerrado-Amazon transition. **Tropical and Subtropical Agroecosystems**, v. 23, n. 2, p. 1-13, 2020a.

BORELLA, D. R.; SOUZA, A. P. de; SILVA, A. C. da; FELIPE, R. T. A.; SILVA, K. N. C.; SOUZA, J. H. G. DE. Thermal requirements and filocron of *Dipteryx alata* under shading levels in the Cerrado Amazon transtition. **Scientia Plena**, v. 16, n. 5, p. 1-15, 2020b. DOI: 10.14808/sci.plena.2020.051702

BORELLA, D. R.; SOUZA, A. P. de; SILVA, K. N. C.; SANTOS, L. M. M dos; XIMENES, E. S. O. C.; ANJOS, A. M. dos. Dynamics and estimates of air temperature and relative humidity in nurseries protected with different shading. **Nativa**, v. 9, n. 1, p. 62-75, 2021. DOI: 10.31413/nativa.v9i1.11437

CHOAB, N.; ALLOUHIB, A.; EL MAAKOULC, A.; KOUSKSOUD, T.; SAADEDDINEA, S.; JAMIL, A. Review on greenhouse microclimate and application: Design parameters, thermal modeling and simulation, climate controlling technologies. **Solar Energy**, v. 191, p. 109-137, 2019. DOI: 10.1016/j.solener.2019.08.042

ESCOBEDO, J. F.; GOMES, E. N.; OLIVEIRA, A. P.; SOARES, J. Modeling hourly and daily fractions of UV, PAR and NIR to global solar radiation under various sky conditions at Botucatu, Brazil. **Applied Energy**, v. 86, n. 3, p. 299-309, 2009. DOI: 10.1016/j.apenergy.2008.04.013

HOLCMAN, E.; SENTELHAS. P. C. Microclimate under different shading screens in greenhouses cultivated with bromeliads. **Revista Brasileira de Engenharia Agrícola e Ambiental**, v. 16, n. 8, p. 858-863, 2012.

KOTILAINEN, T.; ROBSON, T. M.; HERNÁNDEZ, R. Light quality characterization under climate screens and shade nets for controlled-environment agriculture. **PLoS ONE**, v. 13, n. 6, e0199628, p. 1-22, 2018. DOI: 10.1371/journal.pone.0199628

MAHMOOD, A.; HU, Y.; TANNY, J.; ASANTE, E. A. Effects of shading and insect-proof screens on crop microclimate and production: A review of recent advances. **Scientia Horticulturae**, v. 241, p. 241-251, 2018. DOI: 10.1016/j.scienta.2018.06.078

MONTEIRO, E. B.; SILVA, A. C. da; SOUZA, A. P. de; TANAKA, A. A.; FERNEDA, B. G.; MARTIM, C. C. Water requirements and crop coefficients of tropical forest seedlings in different shading conditions. **Revista Brasileira de Engenharia Agrícola e Ambiental**, v. 20, n. 8, p. 709-715, 2016. DOI: 10.1590/1807-1929/agriambi.v20n8p709-715

PALÁCIOS, R. S.; SALLO, F. da S.; MARQUES, J. B.; SANTOS, A. C. A.; MENEZES, J. A.; BIUDES, M. S.; NOGUEIRA, J. de S. Spatiotemporal variability of the optical depth of aerosols in areas of the savannah and of the Pantanal in the central region of Brazil. **Nativa**, v. 6, n. 1, p. 56-65, 2018. DOI: 10.31413/nativa.v6i1.5153

ROSSI, T. J.; ESCOBEDO, J. F.; SANTOS, C. M.; ROSSI, L. R.; SILVA, M. B. P.; DAL PAI, E. Global, diffuse and direct solar radiation of the infrared spectrum in Botucatu/SP/Brazil. **Renewable and Sustainable Energy Reviews**, v. 82, p. 448- 459, 2018. DOI: 10.1016/j.rser.2017.09.030

SABINO, M.; FERNEDA, B. G.; MARTIM, C. C.; BOUVIÉ, L.; SILVA, C. C. da; SOUZA, A. P. de; SILVA, A. C. da; FELIPE, R. T. A. Initial growth of amazonian and brazilian Cerrado yellow ipe cultivated under different shading intensities and spectral wavelength. **Interciência**, v. 45, n. 4, p. 183-191, 2020.

SOUZA, A. P. de; MOTA, L. L. da; ZAMADEI, T.; MARTIM, C. C.; ALMEIDA, F. T. de; PAULINO, J. Climate classification and climatic water balance in Mato Grosso state Brazil. **Nativa**, v. 1, n. 1. p. 34-43, 2013. DOI: 10.31413/nativa.v1i1.1334

SOUZA, A. P. de; ZAMADEI, T.; MONTEIRO, E. B.; CASAVECCHIA, B. H. Atmospheric Transmissivity of the Global Radiation in the Amazonic Region of Mato Grosso. **Revista Brasileira de Meteorologia**, v. 31, n. 4 (suppl.), p. 639-648, 2016. DOI: 10.1590/0102-7786312314b20150147

SOUZA, A. P. de; SILVA, A. C. da; TANAKA, A. A.; ULIANA, E. M.; ALMEIDA, F. T. de; KLAR, A. E.; GOMES, A. W. A. Global radiation by simplified models for the state of Mato Grosso Brazil. **Pesquisa Agropecuária Brasileira**, v. 52, n. 4, p. 215-227, 2017. DOI: 10.1590/S0100-204X2017000400001

STATUTO, D.; ABDEL-GHANY, A. M.; STARACE, G.; ARRIGONI, P.; PICUNO, P. Comparison of the Efficiency of Plastic Nets for Shading Greenhouse in Different Climates. In: COPPOLA, A.; DI RENZO, G.; ALTIERI, G.; D'ANTONIO, P. (eds) **Innovative Biosystems Engineering for Sustainable Agriculture, Forestry and Food Production**. In: International Mid-Term Conference 2019 of the Italian Association of Agricultural Engineering (AIIA), v. 67. p. 287-294, 2020. DOI: 10.1007/978-3-030-39299-4_33

TANG, Y.; MA, X.; LI, M.; WANG, Y. The effect of temperature and light on strawberry production in a solar greenhouse. **Solar Energy**, v. 195, p. 318-328, 2020. DOI: 10.1016/j.solener.2019.11.070

TERAMOTO, E. T.; SILVA E CUNHA, D. C. da; SANTOS, C. M. dos; MACHADO, L. P.; ESCOBEDO, J. F. Estimating daily global radiation from common meteorological variables in a humid subtropical environment. **Nativa**, v. 7, n. 6, p. 693-701, 2019. DOI: 10.31413/nativa.v7i6.7948

WANG, X. Y.; XU, X. M.; CUI, J. The importance of blue light for leaf area expansion, development of photosynthetic apparatus, and chloroplast ultrastructure of Cucumis sativus grown under weak light. **Photosynthetica**, v. 53, n. 2, p. 213-222, 2015. DOI: 10.1007/s11099-015-0083-8

WU, A.; HAMMER, G. L.; DOHERTY, A.; CAEMMERER, S. VON; FARQUHAR, G. D. Quantifying impacts of enhancing photosynthesis on

crop yield. **Nature Plants**, v. 5, p. 380-388, 2019. DOI: 10.1038/s41477-019-0398-8

ZAMADEI, T.; SOUZA, A. P. de; ESCOBEDO, J. F.; ALMEIDA, F. T. de. Estimation of daily diffuse radiation based on atmospheric transmissivity and insolation ratio in the Cerrado-Amazon transition. **Revista Brasileira de Climatologia**, v. 23, p. 134-151, 2018. DOI: 10.5380/abclima.v23i0

ZAMADEI, T.; SOUZA, A. P. de; ALMEIDA, F. T. de.; ESCOBEDO, J. F. Daily Global and diffuse radiation in the Brazilian Cerrado-Amazon transition region. **Ciência e Natura**, v. 43, e37, p. 1-20, 2021. DOI: 10.5902/2179460X39775

ZHANG, S. B.; ZHANG, J. L. Variations in light energy dissipation in Woodfordia fruticosa leaves during expansion. **Photosynthetica**, v. 55, n. 4, p. 705-715, 2017. DOI: 10.1007/s11099-017-0692-5